Published in final edited form as:
Biochim Biophys Acta. 2016 June ; 1862(6): 1111–1121. doi:10.1016/j.bbadis.2016.02.007.

Involvement of connexin43 in acetaminophen-induced liver injury

Michaël Maes[1], **Mitchell R. McGill**[2,#], **Tereza Cristina da Silva**[3], **Chloé Abels**[4], **Margitta Lebofsky**[2], **Cintia Maria Monteiro de Araújo**[3], **Taynã Tiburcio**[3], **Isabel Veloso Alves Pereira**[3], **Joost Willebrords**[1], **Sara Crespo Yanguas**[1], **Anwar Farhood**[5], **Alain Beschin**[4], **Jo A. Van Ginderachter**[4], **Maria Lucia Zaidan Dagli**[3], **Hartmut Jaeschke**[2], **Bruno Cogliati**[3,*], and **Mathieu Vinken**[1,*]

[1]Department of *In Vitro* Toxicology and Dermato-Cosmetology, Vrije Universiteit Brussel, Brussels, Belgium

[2]Department of Pharmacology, Toxicology and Therapeutics, University of Kansas Medical Center, Kansas City, United States of America

[3]Department of Pathology, School of Veterinary Medicine and Animal Science, University of São Paulo, São Paulo, Brazil

[4]Myeloid Cell Immunology, VIB, Brussels, Belgium; Cellular and Molecular Immunology Research Group, Vrije Universiteit Brussel, Brussels, Belgium

[5]Department of Pathology, St. David's North Austin Medical Center, Austin, United States of America

Abstract

Background and aims—Being goalkeepers of liver homeostasis, gap junctions are also involved in hepatotoxicity. However, their role in this process is ambiguous, as gap junctions can act as both targets and effectors of liver toxicity. This particularly holds true for drug-induced liver insults. In the present study, the involvement of connexin 26, connexin32 and connexin43, the building blocks of liver gap junctions, was investigated in acetaminophen-induced hepatotoxicity.

Methods—C57BL/6 mice were overdosed with 300 mg/kg body weight acetaminophen followed by analysis of the expression and localization of connexins as well as monitoring of hepatic gap junction functionality. Furthermore, acetaminophen-induced liver injury was compared between mice genetically deficient in connexin43 and wild type littermates. Evaluation of the toxicological response was based on a set of clinically relevant parameters, including protein adduct formation, measurement of alanine aminotransferase activity, cytokines and glutathione.

Contact information: Mathieu Vinken, Vrije Universiteit Brussel, Department of *In Vitro* Toxicology and Dermato-Cosmetology, Laarbeeklaan 103, B-1090 Brussels, Belgium; Tel: +32-2-4774587; Fax: 32-2-4774582; mvinken@vub.ac.be.
[#]Present address: Department of Pathology and Immunology, Washington University School of Medicine, St. Louis, United States of America
[*]These authors share equal seniorship.

Conflict of interest
The authors declare that the research was conducted in the absence of any commercial or financial relationships that could be construed as a potential conflict of interest.

Europe PMC Funders Author Manuscripts

Results—It was found that gap junction communication deteriorates upon acetaminophen intoxication in wild type mice, which is associated with a switch in mRNA and protein production from connexin32 and connexin26 to connexin43. The upregulation of connexin43 expression is due, at least in part, to *de novo* production by hepatocytes. Connexin43-deficient animals tended to show increased liver cell death, inflammation and oxidative stress in comparison with wild type counterparts.

Conclusion—These results suggest that hepatic connexin43-based signaling may protect against acetaminophen-induced liver toxicity.

Keywords

connexin43; hepatotoxicity; acetaminophen; acute liver injury

1 Introduction

Gap junctions mediate direct intercellular signaling by providing a pathway for the exchange of small (*i.e.* < 1 kDa) and hydrophilic molecules and ions between adjacent cells [1]. In liver, gap junctional intercellular communication (GJIC) among hepatocytes has been found to be essential for a number of critical liver-specific functions, including xenobiotic biotransformation [2–4], glycogenolysis [5–7], secretion of albumin [8], ammonia detoxification [8] and bile secretion [9, 10]. Gap junctions arise from the interaction of 2 hemichannels of neighboring cells, which are themselves composed of 6 connexin (Cx) proteins. More than 20 different connexin proteins have yet been identified in mammals, all which are expressed in a cell-specific way [11]. In healthy liver, hepatocytes mainly produce Cx32 and small quantities of Cx26, while non-parenchymal cells typically express Cx43. However, during liver disease, toxicity, inflammation and oxidative stress, hepatic Cx43 expression increases at the expense of Cx32 and Cx26 [12–18]. Indeed, Cx32 production is drastically downregulated upon acute-on-chronic liver failure in rats. At the same time, Cx43-positive spots appear in particular in the vicinity of inflamed and necrotic areas [19]. Similarly, *de novo* expressed Cx43 in hepatocytes of rats overdosed with acetaminophen (APAP) is co-localized with caspase 3, which may further point to the possible involvement of this connexin species in cell death [20].

The goal of the present study is to gain more insight into the role of Cx43 in hepatotoxicity, particularly APAP-induced liver injury. In a first series of experiments, a detailed scenario is provided of the fate of hepatic Cx26, Cx32 and Cx43 upon APAP overdosing at the transcriptional, translational and activity level. In a second set of studies, APAP-triggered hepatotoxicity is compared between wild type (WT) mice and littermates genetically deficient in Cx43. Evaluation is done based on several mechanistic and clinically relevant read-outs.

2 Methods and materials

2.1 Animals and treatment

Male WT C57BL/6 mice were obtained from Jackson Laboratories (USA). $Cx43^{+/-}$ mice were kindly provided by the International Agency for Research on Cancer (France) [21] and

were backcrossed with WT C57BL/6 mice, and genotype was controlled as previously described [22]. Heterozygous Cx43-deficient mice were used, as the corresponding homozygous null mutation is lethal [21]. The animals were housed in the animal facility of the Department of Pathology, School of Veterinary Medicine and Animal Science of the University of São Paulo. The mice were kept in a room with ventilation (*i.e.* 16-18 air changes/hour), relative humidity (*i.e.* 45-65%), controlled temperature (*i.e.* 20-24°C) and light/dark cycle 12:12, and were given water and balanced diet (NUVILAB-CR1, Nuvital Nutrientes LTDA, Brazil) *ad libitum*. Mice were starved 15 hours *prior* to APAP or vehicle (*i.e.* saline; 0.9% sodium chloride) administration. APAP (Sigma, USA) was dissolved in saline, slightly heated (*i.e.* 30-37°C) and injected intraperitoneally at 300 mg/kg body weight after which animals regained free access to food. A control group was treated with saline in parallel. Mice were euthanized at the start of the experiment, and 1, 6 and 24 hours after APAP or saline injection by exsanguination during sampling under isoflurane-induced anesthesia. Blood, collected by cardiac puncture, was drawn into a heparinized syringe and centrifuged for 10 minutes at 1503x*g*, and serum was stored at -20°C. Livers were excised and fragments were fixed in 10% phosphate-buffered formalin or snap-frozen in liquid nitrogen with storage at -80°C. This study has been approved by the Committee on Bioethics of the School of Veterinary Medicine and Animal Science of the University of São Paulo (protocol number 9999100314), and all animals received humane care according to the criteria outlined in the “Guide for the Care and Use of Laboratory Animals”.

2.2 Connexin mRNA expression analysis

Total RNA was extracted from liver tissue using a GenElute™ Mammalian Total RNA Purification Miniprep Kit (Sigma, USA) and the On-Column DNase I Digestion Set (Sigma, USA) according to the manufacturer’s instructions. Purity and quantification of isolated RNA were measured spectrophotometrically using a NanoDrop® ND-100 Spectrophotometer (Thermo Scientific, USA). A cut-off ratio between 1.8 and 2.1 for the absorption at 260/280 nm was used for assessing purity. Then, 2 μg mRNA was reversely transcribed into cDNA with an iScript™ cDNA Synthesis Kit (Bio-Rad, USA) using an iCycler iQ™ (Bio-Rad, USA) followed by cDNA purification using a GenElute™ PCR Clean-Up Kit (Sigma, USA). cDNA products were quantitatively amplified using Taqman probes and primers (Applied Biosystems, USA) targeted towards Cx26, Cx32 and Cx43 (Table 1). All samples were analyzed in duplicate. Each run included a serial dilution of a pooled cDNA mix from all cDNA samples and 2 no template controls to estimate the quantitative polymerase chain reaction efficiency. For reverse transcription quantitative real-time polymerase chain reaction (RT-qPCR) analysis, a reaction mix was prepared containing TaqMan® Fast Advanced Master Mix (Applied Biosystems, USA) Assay-on-Demand™ Mix Gene Expression Assay Mix (Applied Biosystems, USA) and cDNA diluted in nuclease-free water. The qPCR conditions, using a StepOnePlus™ real-time PCR system (Life Technologies, USA) included incubation for 20 seconds at 95°C followed by 40 cycles of denaturation for 1 second at 95°C and annealing for 20 seconds at 60°C. Efficiency was estimated by StepOnePlus™ system’s software and only data with polymerase chain reaction efficiency between 90% and 110% were used. Stable reference genes for normalization were identified out of a pool of 6 genes as determined by geNorm using the qbase^{+} software (Biogazelle, Belgium) (Table 1) [23]. The resulting ΔCq-values of the test

samples were normalized to those of the calibrator samples, yielding ΔΔCq values. Relative alterations (*i.e.* fold change) in mRNA levels were calculated according to the Livak $2^{-\Delta\Delta Cq}$ formula [24].

2.3 Connexin protein expression analysis

Flash frozen liver tissue was homogenized in radio-immunoprecipitation assay buffer (Thermo Scientific, USA) containing Halt™ protease and phosphatase inhibitor cocktail (Thermo Scientific, USA), and ethylenediaminetetraacetic acid (Thermo Scientific, USA). Following sonication for 30 seconds, samples were rotated for 15 minutes at 4°C. Cell lysates were centrifuged at 14000x*g* for 5 minutes and protein concentrations were determined in the supernatants by means of a bicinchoninic acid assay (Pierce, USA) with bovine serum albumin as a standard. Proteins were separated on 10% (*i.e.* for Cx43 analysis) or 12% (*i.e.* for Cx26 and Cx32 analysis) Mini-Protein® TGX Stain-Free™ precast gels (Bio-Rad, USA) using electrophoresis and blotted onto nitrocellulose Trans-Blot® Turbo™ Transfer packs (Bio-Rad, USA) with activation and quantification of the stain-free loading. Subsequent blocking of the membranes was performed with blocking buffer, 5% non-fatty milk in Tris-buffered saline solution (*i.e.* 20 mM Tris and 135 mM sodium chloride) containing 0.1% Tween-20. Membranes were incubated overnight at 4°C with primary antibody directed against Cx26 (Invitrogen, USA), Cx32 (Sigma, USA) and Cx43 (Sigma, USA), all diluted 1:1000 in blocking buffer followed by incubation for 1 hour at room temperature with polyclonal goat anti-rabbit secondary antibody (Dako, Denmark) diluted 1:1000 in blocking buffer. Excessive antibody was removed by washing the membranes several times in Tris-buffered saline solution containing 0.1% Tween-20. Detection of the proteins was carried out by means of a Pierce™ enhanced chemiluminescence Western blotting substrate kit (Thermo Scientific, USA) according to the manufacturer's instructions. Densitometric analysis was performed using Image Lab 5.0 software (Bio-Rad, USA). For semi-quantification purposes, Cx26, Cx32 and Cx43 signals were normalized against total protein and expressed as relative alterations compared to untreated animals.

2.4 Connexin protein localization analysis

Flash frozen liver tissue samples were embedded in Tissue Freezing Medium® (Leica, UK). Then, 10 μm liver sections were fixed in acetone for 10 minutes at -20°C. Liver sections were incubated with primary antibodies directed against Cx26 (Invitrogen, USA), Cx32 (Sigma, USA) and Cx43 (Sigma, USA), diluted 1:250, 1:500 and 1:100, respectively, in blocking buffer containing phosphate-buffered saline supplemented with 0.1% sodium azide (Sigma, USA) and 1% bovine serum albumin (Sigma, USA) during 1 hour at 37°C. After extensive rinsing with phosphate-buffered saline supplemented with 0.5% Tween-20, samples were incubated with polyclonal goat anti-rabbit Alexa Fluor® 488-conjugated secondary antibody (Life Technologies, USA) diluted 1:500 in blocking buffer. Nuclei were stained with 1 μg/ml propidium iodide (Sigma, USA) and samples were mounted with Vectashield (Vector Laboratories, USA). Detection was performed by fluorescence microscopy (Zeiss, Germany).

Europe PMC Funders Author Manuscripts

2.5 Isolation of hepatocytes and analysis of connexin43 expression

Male 8-weeks old WT C57BL/6 mice were obtained from Janvier (France). The animals were housed at the Laboratory of Cellular and Molecular Immunology at the Vrije Universiteit Brussel. Mice were starved 15 hours *prior* to APAP administration. APAP (Sigma, USA) was dissolved in saline, slightly heated and injected intraperitoneally at 300 mg/kg body weight after which animals regained free access to food. Mice were euthanized at 6 and 24 hours after APAP injection by carbon dioxide. For the isolation of hepatocytes, livers were prelevated after perfusion with phosphate-buffered saline, chopped finely and incubated for 20 minutes with 1 mg/ml collagenase A (Sigma, USA) and 10 IU/ml DNase (Roche, Germany) in a shaking water bath at 37°C. After filtration through a 70 μm filter, cells were centrifuged at 400x*g* and 4°C for 5 minutes. Red blood cells were lyzed with 8.3 g/L NH_4Cl in 10 mM Tris-buffer. Then, 10^6 cells were stained with fluorescein isothiocyanate-conjugated anti-hepatocyte cell adhesion molecule (hepaCAM) antibody (Bioss, USA) and allophycocyanin cyanine 7-labeled pan anti-cluster of differentiation (CD) 45 antibody (BioLegend, USA) at 4°C for 20 minutes, washed and subsequently fixed and permeabilized with Cytofix/Cytoperm™ (BD Biosciences, USA), following the manufacturer's instructions. The fixed cells were stained with primary anti-Cx43 antibody (Sigma, USA) at 4°C for 20 minutes, washed and incubated at 4°C for 20 minutes with DyLight™ 405-conjugated secondary antibody (Jackson ImmunoResearch, USA) and subjected to flow cytometry. The results were analyzed with a FACScantoII (BD Biosciences, USA) and FlowJo software (TreeStar, USA). Hepatocytes were detected as live-gated hepaCAM$^+$ CD45$^-$ cells. All experiments were carried out in accordance with the guidelines provided by the ethical committee on animal experimentation of the Vrije Universiteit Brussel.

2.6 Gap junction activity analysis

GJIC was studied by means of an *ex vivo* incision loading/dye transfer assay [25] with some modifications [26]. Immediately after euthanasia of the mice, part of the left hepatic lobe was excised. Incisions were made on the surface and 0.5% Lucifer Yellow (Sigma, USA) in phosphate-buffered saline was dropped into the tissue surface and incubated for 3 minutes. After washing with phosphate-buffered saline, liver fragments were fixed in 10% buffered formalin and embedded in paraffin. Subsequently, 5 μm sections were deparaffinized and studied under a fluorescence microscope (Nikon, Japan). Dye transfer was analyzed using the ImagePro-Plus system version 4.5 (Media Cybernetics, USA) and GJIC was assessed by calculating the ratio between the area of diffused Lucifer Yellow and length of incision.

2.7 Analysis of hepatic protein adducts

APAP-protein adducts were measured by high-pressure liquid chromatography with electrochemical detection as previously described [27] with some modifications [28]. Briefly, protein samples were filtered through size exclusion columns *prior* to digestion with proteases and the protein-derived APAP-cysteine conjugates were quantified and normalized to protein concentration in the original samples.

2.8 Analysis of serum alanine aminotransferase

Alanine aminotransferase (ALT) was measured with an automated spectrophotometric Labmax 240 analyzer (Labtest Diagnostica, Brazil) after appropriate dilution of serum samples. Values were expressed in IU/L.

2.9 Histopathological liver examination

For microscopic examination of liver tissue, formalin-fixed liver fragments were embedded in paraffin, and 5 μm sections were cut and stained with hematoxylin-eosin. Pictures were taken using a KF2 microscope (Zeiss, Germany).

2.10 Analysis of liver and serum cytokines

Liver tissue was homogenized in lysis buffer with protease inhibitors (Roche, Germany). Homogenates were centrifuged at 14000x*g* for 15 minutes at 4°C and protein concentrations in supernatants were determined according to the Bradford procedure [29] using a commercial kit (Bio-Rad, USA) with bovine serum albumin as a standard. Enzyme-linked immunosorbent assay (ELISA) kits were used to measure levels of mouse interleukin (IL)-1β, IL-6, IL-10, interferon γ (IFNγ) and tumor necrosis factor α (TNFα) (BD Biosciences, USA). Wells of a 96-well plate were coated overnight with appropriate monoclonal antibody diluted in coating buffer and blocked for 1 hour with phosphate-buffered saline containing fetal bovine serum. Subsequently, wells were incubated with liver homogenate, serum or standard solution for 2 hours, followed by incubation with appropriate biotinylated monoclonal antibody and streptavidin-horseradish peroxidase conjugate for 1 hour and 30 minutes, respectively. Finally, wells were exposed to tetramethylbenzidine substrate reagent for 30 minutes. The reaction was stopped by adding phosphoric acid and absorbance was measured at 450 nm with wavelength correction at 570 nm using a Varioskan™ Flash Multimode Reader (Thermo Scientific, USA).

2.11 Hepatic glutathione and glutathione disulfide analysis

GSH and glutathione disulfide (GSSG) levels in liver tissue were measured using a modified Tietze assay [30]. Briefly, frozen liver tissue was homogenized in 3% sulfosalicylic acid/ethylendiaminetetraacetic acid and centrifuged at 18000x*g* for 5 minutes at 4°C to remove precipitated proteins. After further dilution with potassium phosphate buffer, samples were assayed with a cycling reaction utilizing GSH reductase and dithionitrobenzoic acid. Measurement of GSSG was performed using the same method after trapping GSH with *N*-ethylmaleimide and removal by solid phase extraction [30]. GSSG content was expressed as GSH equivalents.

2.12 Statistical analysis

The number of repeats (n) for each analysis varied and is specified in the discussion of the results. All data were expressed as mean ± standard error of the mean (SEM). Results were statistically processed by 1-way analysis of variance (ANOVA) followed by *post hoc* Bonferroni tests using GraphPad Prism6 software with probability (*p*) values of less than or equal to 0.05 considered as significant.

3 Results

3.1 Effects of APAP toxicity on hepatic connexin expression

In rat liver, about 90% of the total connexin amount is due to Cx32, while Cx26 and Cx43 each account for 5% of hepatic connexin abundance [31, 32]. Several groups described that hepatic Cx43 production increases at the expense of Cx32 and Cx26 in stressful situations [19, 20, 33]. Indeed, Cx43 protein levels were significantly elevated ($p \leq 0.0001$) already 6 hours after APAP administration and peaked at 24 hours. Cx43 was detected as 3 signals, representing the non-phosphorylated and 2 phosphorylated variants (Fig. 1A). The increased total Cx43 protein levels were associated with significantly upregulated Cx43 mRNA quantities at both time points ($p \leq 0.001$ and $p \leq 0.01$, respectively) (Fig. 1B), suggesting that induction of Cx43 expression in APAP toxicity is regulated transcriptionally. On the other hand, Cx32 steady-state protein levels already significantly decreased ($p \leq 0.05$) 1 hour following APAP overdosing, which gradually continued towards 24 hours (Fig. 1C). This was not entirely paralleled in the mRNA profile, as significantly downregulated ($p \leq 0.01$) Cx32 gene transcription only became manifested 6 hours after APAP administration (Fig. 1D). This could suggest that deterioration of Cx32 production in APAP toxicity is primarily controlled by changes in protein turnover and transcription. A similar downregulation was observed for Cx26, with protein levels significantly decreased 1 hour ($p \leq 0.05$), 6 hours ($p \leq 0.0001$) and 24 hours ($p \leq 0.001$) after APAP overdosing (Fig. 1E). In contrast, Cx26 mRNA levels were increased 6 hours after APAP administration (Fig. 1F), which could point to a compensatory effect at the transcriptional level following changes in protein turnover.

3.2 Effects of APAP toxicity on hepatic connexin localization

In normal liver, both Cx32 and Cx43 are evenly distributed in the different acinar areas, whereas Cx26 is preferentially expressed at the periportal acinar pool [34–36]. Although predominantly located at the plasma membrane surface, a considerable portion of the connexin population resides in the cytoplasm of cells, which may reflect the rapid turnover of these proteins found *in vitro* [37] and *in vivo* [38]. In hepatocytes, Cx32-containing gap junctions occupy about 3% of the membrane area [39]. This appears as a dotted pattern upon immunostaining, which was also seen in the present study for both Cx32 and Cx26 (Fig. 2A,B). In line with the results of the immunoblot analysis, subtle changes in Cx32 immunosignals were observed 1 hour after APAP treatment, while disappearance of Cx32-positive spots at cell borders within the injured areas was detected after 6 and 24 hours. Similar observations were made for Cx26, yet this connexin species also disappeared in the non-injured areas (Fig. 2A,B). In contrast, and complying with the immunoblot and RT-qPCR analyses, Cx43 immunoreactivity began to increase 6 hours following APAP overdosing. Cx43 protein was observed in the membrane area, but mainly in the intracellular compartment of liver cells in the injured area after 24 hours (Fig. 2B). As Cx43 is not naturally occurring in hepatocytes, immunostaining suggested possible *de novo* expression of Cx43 in hepatocytes after APAP administration (Fig. 2B). To further verify this observation, livers of APAP-treated and control mice were subjected to flow cytometric analysis, thereby relying on a hepatocyte-specific marker, namely hepaCAM, as well as a hematopoietic cell-specific marker, in particular CD45. This analysis showed initiation of Cx43 expression in hepatocytes, defined as the hepaCAM^{+} CD45^{-} liver cell population, after

APAP-overdosing (Fig. 3), which is in line with the results of the immunohistochemistry analysis (Fig. 2B).

3.3 Effects of APAP toxicity on hepatic gap junction activity

The occurrence of gap junctions between non-parenchymal liver cells still is a matter of debate despite the established expression of Cx43 in these cells. This is in contrast to hepatocytes, which are abundantly coupled with each other, mainly through Cx32-based gap junctions [40]. Therefore, the latter are believed to account for the vast majority of GJIC activity in liver. This is substantiated by the findings of the present study, showing significantly decreased ($p \leq 0.05$) gap junction coupling based on dye transfer starting 6 hours after APAP administration (Fig. 4), which is preceded by a drop in Cx32 protein levels. These results also demonstrate that Cx43, although strongly upregulated in APAP toxicity, cannot functionally compensate for the loss of Cx32 and thus further shows that this connexin species, which is partly located in the cytoplasm of liver cells (Fig. 2B), is unlikely to participate in overall hepatic GJIC.

3.4 Effects of Cx43 ablation on connexin protein content during APAP toxicity

To investigate whether the upregulation of Cx43 is actively involved in APAP toxicity, whole body $Cx43^{+/-}$ mice were used in the next set of experiments. Homozygous $Cx43^{-/-}$ mice are not viable [21] and hence heterozygous counterparts were used in this study. Thus, WT and $Cx43^{+/-}$ mice were overdosed with APAP followed by sampling at different time points. Cx43 protein content in the $Cx43^{+/-}$ animals was consistently reduced compared to WT littermates. Specifically, the Cx43 amount in $Cx43^{+/-}$ mice was 28 ± 11% at 0 hours, 37 ± 13% at 1 hour, 32 ± 19% at 6 hours and 35 ± 10% at 24 hours of the Cx43 abundance in WT counterparts (Fig. 5A). These results reinforce the use of $Cx43^{+/-}$ mice as a negative control for Cx43 signaling in APAP-induced hepatotoxicity. Furthermore, no differences were detected in Cx32 protein levels between $Cx43^{+/-}$ and WT mice after APAP administration (Fig. 5B).

3.5 Effects of Cx43 ablation on hepatic protein adduct formation during APAP toxicity

APAP-induced hepatotoxicity depends on biotransformation mediated by cytochrome P450 2E1, yielding the deleterious metabolite NAPQI [41]. Under normal circumstances, NAPQI can be rapidly detoxified by binding to GSH. However, in case of APAP overdosing, GSH becomes depleted and NAPQI can react with protein sulfhydryl groups, which leads to the formation of noxious liver protein adducts [42]. In this respect, APAP-protein adducts were clearly detectable in all mice already 1 hour after APAP administration. At 6 hours, no differences were observed in $Cx43^{+/-}$ mice compared to WT animals (Fig. 6).

3.6 Effects of Cx43 ablation on hepatic cell death during APAP toxicity

The formation of APAP-protein adducts in APAP toxicity ultimately burgeons into the onset of massive hepatocyte cell death, which typically occurs in a zonated pattern. Specifically, necrotic patches appear around the central vein, where expression of cytochrome P450 enzymes responsible for NAPQI formation is highest [43, 44]. In the current study, histopathological analysis did not reveal liver injury 1 hour after APAP overdosing (data not

shown). The necrotic areas became increasingly detectable microscopically 6 hours after administration of APAP to $Cx43^{+/-}$ and WT mice (Fig. 7A). This is associated with the increased presence of ALT in serum. This cytosolic enzyme leaks from the cell into the serum upon membrane damage, which occurs in case of necrosis [45]. In all animals tested in this study, ALT levels were elevated starting 6 hours after APAP administration. After 24 hours, ALT levels were significantly higher ($p \leq 0.01$) in $Cx43^{+/-}$ animals compared to the WT cohort (Fig. 7B).

3.7 Effects of Cx43 ablation on hepatic inflammation during APAP toxicity

APAP overdosing triggers the inflammatory machinery, which partly relies on non-parenchymal liver cells and that is associated with the activation of a plethora of pro-inflammatory and anti-inflammatory cytokines [46–50]. However, in this study, only subtle changes in hepatic levels of the prototypical pro-inflammatory cytokines IL-1β and TNFα were recorded in the 24 hours timeframe following APAP administration to WT animals (Fig. 8). By contrast, IL-1β and TNFα levels gradually increased in APAP-treated $Cx43^{+/-}$ mice and were significantly higher ($p \leq 0.0001$) than those observed in WT animals at 24 hours. This effect was only seen in liver and not in serum, where levels were below the detection limit for all study groups at the start of APAP administration and after 1 hour. Hepatic profiles of IL-6 were similar in all animals, with a clear peak 1 day posttreatment and no differences between the test groups (Fig. 8). This was unlike anti-inflammatory IL-10, which tended to progressively increase in livers of WT animals, but not $Cx43^{+/-}$ mice ($p \leq 0.01$) 6 hours after APAP overdosing, followed by a steep decline at 24 hours. Interestingly, IL-10 behaved in the opposite way in serum, with an increase from 6 to 24 hours following APAP treatment in all conditions. This specifically holds true for $Cx43^{+/-}$ mice, whose IL-10 serum levels were significantly higher ($p \leq 0.01$) at 24 hours compared to WT animals (Fig. 8). Serum levels of IFNγ were below the detection limit (data not shown). Increased amounts of hepatic IFNγ were found in $Cx43^{+/-}$ mice at 24 hours ($p \leq 0.01$) compared to WT mice at specific time points (Fig. 8).

3.8 Effects of Cx43 ablation on hepatic oxidative stress during APAP toxicity

Several mechanisms underlie oxidative stress associated with APAP toxicity, with a prominent one being GSH depletion due to excessive NAPQI production [51, 52]. In this study, a reduction in the GSH pool indeed became evident 1 hour after APAP overdosing of all mice. This was followed by a recovery at 24 hours, which was, however, significantly lower ($p \leq 0.0001$) in $Cx43^{+/-}$ mice (Fig. 9A). GSH acts as a critical anti-oxidant and is converted to its oxidized GSSG form upon reaction with reactive oxygen species. For all experimental groups, GSSG formation peaked 24 hours after APAP administration (Fig. 9B), with gradually increased GSSG/GSH ratios (Fig. 9C). At 24 hours, the GSSG/GSH ratio was significantly elevated ($p \leq 0.001$) in $Cx43^{+/-}$ mice compared to WT animals, suggesting more oxidative stress.

4 Discussion

Because of their important function in liver homeostasis [53], it is not surprising that connexins also play a role in liver toxicity and disease. To address this topic, the present

study specifically focused on liver damage induced by overdose of APAP, a readily available analgesic and antipyretic drug that accounts for the majority of all clinical cases of drug-induced liver injury in Western countries [54, 55]. It was found that a switch from Cx26 and Cx32 to Cx43 expression occurs in liver during APAP intoxication. The upregulation of Cx43 expression is due, at least in part, to *de novo* production by hepatocytes. This seems to be a generic response to insult, as this has also been reported for many other stress situations in the liver both *in vitro* and *in vivo* [33, 56]. Nevertheless, the molecular mechanisms that underlie this process remain elusive. The findings of this study suggest that Cx43 presence in APAP overdosing is regulated at the transcriptional level. In this respect, Cx43 gene expression is known to be controlled by the transcription factor activator protein-1, which is composed of the proto-oncogenes *c*-fos and *c*-jun [57]. In rat myometrium, activator protein-1 has been shown to induce Cx43 expression under stress conditions [58]. It is conceivable that a similar scenario takes place in the liver during APAP intoxication. Indeed, increased *c*-jun mRNA transcript levels and enhanced DNA binding of activator protein-1 have been observed in mouse liver following administration of toxic doses of APAP [59]. In addition, inflammatory conditions, such as exposure to lipopolysaccharide and IFNγ, have been found to increase Cx43 mRNA and protein amounts in Kupffer cells *in vitro* and *in vivo* [13]. Increased Cx43 levels may also reflect migration of oval cells into damaged areas. These stem cell-like progenitor cells, which can differentiate into hepatocytes or biliary epithelial cells, express Cx43 in early phases of proliferation [60–63]. Previous studies have shown the involvement of oval cells in the regenerative process after chemical-induced hepatotoxicity in rodents [60, 64, 65]. On the other hand, the observed downregulation of Cx32 production in APAP-induced liver toxicity may be driven by both altered protein turnover and transcriptional mechanisms, while Cx26 downregulation seems primarily regulated at the translational level. In fact, oxidative stress and inflammation have been repeatedly reported to negatively affect Cx26 and Cx32 protein and/or mRNA expression in liver [14–18]. Collectively, these drastic modifications in connexin expression profiles result in deterioration of GJIC. This implies that despite its boosted production, Cx43 cannot maintain gap junction activity in liver during APAP toxicity. This is further substantiated by immunohistochemical data showing that Cx43 is mainly found in the cytoplasm of liver cells. In order to shed more light onto the actual functional relevance of Cx43 upregulation, mice genetically deficient in Cx43 were used in the second part of this study. No differences in early GSH depletion were detected between study groups, indicating that Cx43 ablation does not have a relevant impact on reactive metabolite formation after APAP-overdosing. This was confirmed by monitoring of APAP-protein adduct formation, which showed no major differences between $Cx43^{+/-}$ and WT mice. Furthermore, it was found that hepatic GSH recovery is delayed in $Cx43^{+/-}$ animals. Since all groups had similar elevated hepatic GSSG levels, the GSSG/GSH ratio was higher in $Cx43^{+/-}$ mice, which is indicative of more pronounced oxidative stress in these animals. In this regard, GSH can scavenge NAPQI and reactive oxygen species, thereby reducing cell stress and damage [66–69]. The postponed GSH recovery could account for the elevated liver injury in $Cx43^{+/-}$ mice, as shown by increased serum ALT quantities and elevated liver levels of the pro-inflammatory cytokines IL-1β, TNFα and IFNγ 24 hours after APAP overdosing. Overall, these data suggest that newly synthesized Cx43 may protect against APAP-induced liver injury.

Acknowledgements

The authors wish to thank Miss Tineke Vanhalewyn, Miss Dinja De Win, Miss Shirlei Meire da Silva, Mister José Alexandre Coelho Pimentel and Mister Paul Claes for their dedicated technical assistance. This work was financially supported by the grants from the Agency for Innovation by Science and Technology in Flanders (IWT), the European Research Council (ERC Starting Grant 335476), the Fund for Scientific Research-Flanders (FWO grants G009514N and G010214N), the University Hospital of the Vrije Universiteit Brussel-Belgium ("Willy Gepts Fonds" UZ-VUB), the US National Institutes of Health (R01 DK102142), the University of São Paulo-Brazil and the Foundation for Research Support of the State of São Paulo (FAPESP SPEC grant 2013/50420-6).

List of abbreviations

ALT	alanine aminotransferase
APAP	acetaminophen
CD	cluster of differentiation
Cx	connexin
ELISA	enzyme-linked immunosorbent assay
GJIC	gap junctional intercellular communication
GSH	glutathione
GSSG	glutathione disulfide
hepaCAM	hepatocyte cell adhesion molecule
IFNγ	interferon γ
IL-1β/6/10	interleukin 1β/6/10
n	number of repeats
NAPQI	*N*-acetyl-*p*-benzoquinone imine
p	probability
RT-qPCR	reverse transcription quantitative real-time polymerase chain reaction
SEM	standard error of the mean
TNFα	tumor necrosis factor α
WT	wild type

References

[1]. Alexander DB, Goldberg GS. Transfer of biologically important molecules between cells through gap junction channels. Curr Med Chem. 2003; 10:2045–2058. [PubMed: 12871102]

[2]. Neveu MJ, Babcock KL, Hertzberg EL, Paul DL, Nicholson BJ, Pitot HC. Colocalized alterations in connexin32 and cytochrome P450IIB1/2 by phenobarbital and related liver tumor promoters. Cancer Res. 1994; 54:3145–3152. [PubMed: 8205533]

[3]. Shoda T, Mitsumori K, Onodera H, Toyoda K, Uneyama C, Imazawa T, Hirose M. The relationship between decrease in Cx32 and induction of P450 isozymes in the early phase of clofibrate hepatocarcinogenesis in the rat. Arch Toxicol. 1999; 73:373–380. [PubMed: 10550479]

[4]. Shoda T, Mitsumori K, Onodera H, Toyoda K, Uneyama C, Takada K, Hirose M. Liver tumor-promoting effect of beta-naphthoflavone, a strong CYP 1A1/2 inducer, and the relationship between CYP 1A1/2 induction and Cx32 decrease in its hepatocarcinogenesis in the rat. Toxicol Pathol. 2000; 28:540–547. [PubMed: 10930040]

[5]. Stumpel F, Ott T, Willecke K, Jungermann K. Connexin 32 gap junctions enhance stimulation of glucose output by glucagon and noradrenaline in mouse liver. Hepatology. 1998; 28:1616–1620. [PubMed: 9828226]

[6]. Clair C, Chalumeau C, Tordjmann T, Poggioli J, Erneux C, Dupont G, Combettes L. Investigation of the roles of Ca(2+) and InsP(3) diffusion in the coordination of Ca(2+) signals between connected hepatocytes. J Cell Sci. 2001; 114:1999–2007. [PubMed: 11493636]

[7]. Nelles E, Butzler C, Jung D, Temme A, Gabriel HD, Dahl U, Traub O, Stumpel F, Jungermann K, Zielasek J, Toyka KV, et al. Defective propagation of signals generated by sympathetic nerve stimulation in the liver of connexin32-deficient mice. Proc Natl Acad Sci U S A. 1996; 93:9565–9570. [PubMed: 8790370]

[8]. Yang J, Ichikawa A, Tsuchiya T. A novel function of connexin 32: marked enhancement of liver function in a hepatoma cell line. Biochem Biophys Res Commun. 2003; 307:80–85. [PubMed: 12849984]

[9]. Temme A, Stumpel F, Sohl G, Rieber EP, Jungermann K, Willecke K, Ott T. Dilated bile canaliculi and attenuated decrease of nerve-dependent bile secretion in connexin32-deficient mouse liver. Pflugers Arch. 2001; 442:961–966. [PubMed: 11680630]

[10]. Nathanson MH, Rios-Velez L, Burgstahler AD, Mennone A. Communication via gap junctions modulates bile secretion in the isolated perfused rat liver. Gastroenterology. 1999; 116:1176–1183. [PubMed: 10220510]

[11]. Söhl G, Willecke K. An update on connexin genes and their nomenclature in mouse and man. Cell Commun Adhes. 2003; 10:173–180. [PubMed: 14681012]

[12]. Vinken M. Gap junctions and non-neoplastic liver disease. J Hepatol. 2012; 57:655–662. [PubMed: 22609308]

[13]. Eugenin EA, Gonzalez HE, Sanchez HA, Branes MC, Saez JC. Inflammatory conditions induce gap junctional communication between rat Kupffer cells both in vivo and in vitro. Cell Immunol. 2007; 247:103–110. [PubMed: 17900549]

[14]. Yamamoto T, Kojima T, Murata M, Takano K, Go M, Chiba H, Sawada N. IL-1beta regulates expression of Cx32, occludin, and claudin-2 of rat hepatocytes via distinct signal transduction pathways. Exp Cell Res. 2004; 299:427–441. [PubMed: 15350541]

[15]. De Maio A, Gingalewski C, Theodorakis NG, Clemens MG. Interruption of hepatic gap junctional communication in the rat during inflammation induced by bacterial lipopolysaccharide. Shock. 2000; 14:53–59. [PubMed: 10909894]

[16]. Gingalewski C, Wang K, Clemens MG, De Maio A. Posttranscriptional regulation of connexin 32 expression in liver during acute inflammation. J Cell Physiol. 1996; 166:461–467. [PubMed: 8592007]

[17]. Morsi AS, Godfrey RE, Chipman JK, Minchin SD. Characterisation of the connexin32 promoter and changes in response element complexes in rat liver and hepatocytes during culture associated with oxidative stress. Toxicol In Vitro. 2003; 17:191–199. [PubMed: 12650673]

[18]. Kojima T, Mitaka T, Mizuguchi T, Mochizuki Y. Effects of oxygen radical scavengers on connexins 32 and 26 expression in primary cultures of adult rat hepatocytes. Carcinogenesis. 1996; 17:537–544. [PubMed: 8631141]

[19]. Balasubramaniyan V, Dhar DK, Warner AE, Vivien Li WY, Amiri AF, Bright B, Mookerjee RP, Davies NA, Becker DL, Jalan R. Importance of Connexin-43 based gap junction in cirrhosis and acute-on-chronic liver failure. J Hepatol. 2013; 58:1194–1200. [PubMed: 23376361]

[20]. Naiki-Ito A, Asamoto M, Naiki T, Ogawa K, Takahashi S, Sato S, Shirai T. Gap junction dysfunction reduces acetaminophen hepatotoxicity with impact on apoptotic signaling and connexin 43 protein induction in rat. Toxicol Pathol. 2010; 38:280–286. [PubMed: 20097795]

[21]. Reaume AG, de Sousa PA, Kulkarni S, Langille BL, Zhu D, Davies TC, Juneja SC, Kidder GM, Rossant J. Cardiac malformation in neonatal mice lacking connexin43. Science. 1995; 267:1831–1834. [PubMed: 7892609]

[22]. Cogliati B, Vinken M, Silva TC, Araújo CM, Aloia TP, Chaible LM, Mori CM, Dagli ML. Connexin 43 deficiency accelerates skin wound healing and extracellular matrix remodeling in mice. J Dermatol Sci. 2015; 79:50–56. [PubMed: 25900674]

[23]. Vandesompele J, De Preter K, Pattyn F, Poppe B, Van Roy N, De Paepe A, Speleman F. Accurate normalization of real-time quantitative RT-PCR data by geometric averaging of multiple internal control genes. Genome Biol. 2002; 3:research0034. [PubMed: 12184808]

[24]. Livak KJ, Schmittgen TD. Analysis of relative gene expression data using real-time quantitative PCR and the 2(-Delta Delta C(T)) Method. Methods. 2001; 25:402–408. [PubMed: 11846609]

[25]. Sai K, Kanno J, Hasegawa R, Trosko JE, Inoue T. Prevention of the down-regulation of gap junctional intercellular communication by green tea in the liver of mice fed pentachlorophenol. Carcinogenesis. 2000; 21:1671–1676. [PubMed: 10964098]

[26]. da Silva TC, Cogliati B, da Silva AP, Fukumasu H, Akisue G, Nagamine MK, Matsuzaki P, Haraguchi M, Górniak SL, Dagli ML. Pfaffia paniculata (Brazilian ginseng) roots decrease proliferation and increase apoptosis but do not affect cell communication in murine hepatocarcinogenesis. Exp Toxicol Pathol. 2010; 62:145–155. [PubMed: 19427770]

[27]. Muldrew KL, James LP, Coop L, McCullough SS, Hendrickson HP, Hinson JA, Mayeux PR. Determination of acetaminophen-protein adducts in mouse liver and serum and human serum after hepatotoxic doses of acetaminophen using high-performance liquid chromatography with electrochemical detection. Drug Metabol Dispos. 2002; 30:446–451.

[28]. McGill MR, Lebofsky M, Norris HRK, Slawson MH, Bajt ML, Xie YC, Williams CD, Wilkins DG, Rollins DE, Jaeschke H. Plasma and liver acetaminophen-protein adduct levels in mice after acetaminophen treatment: Dose-response, mechanisms, and clinical implications. Toxicol Appl Pharmacol. 2013; 269:240–249. [PubMed: 23571099]

[29]. Bradford MM. A rapid and sensitive method for the quantitation of microgram quantities of protein utilizing the principle of protein-dye binding. Anal Biochem. 1976; 72:248–254. [PubMed: 942051]

[30]. Jaeschke H, Mitchell JR. Use of isolated perfused organs in hypoxia and ischemia/reperfusion oxidant stress. Methods Enzymol. 1990; 186:752–759. [PubMed: 2233332]

[31]. Cascio M, Kumar NM, Safarik R, Gilula NB. Physical characterization of gap junction membrane connexons (hemi-channels) isolated from rat liver. J Biol Chem. 1995; 270:18643–18648. [PubMed: 7629194]

[32]. Neveu MJ, Hully JR, Babcock KL, Vaughan J, Hertzberg EL, Nicholson BJ, Paul DL, Pitot HC. Proliferation-associated differences in the spatial and temporal expression of gap junction genes in rat liver. Hepatology. 1995; 22:202–212. [PubMed: 7601414]

[33]. Vinken M, De Kock J, Oliveira AG, Menezes GB, Cogliati B, Dagli ML, Vanhaecke T, Rogiers V. Modifications in connexin expression in liver development and cancer. Cell Commun Adhes. 2012; 19:55–62. [PubMed: 22950570]

[34]. Berthoud VM, Iwanij V, Garcia AM, Sáez JC. Connexins and glucagon receptors during development of rat hepatic acinus. Am J Physiol. 1992; 263:G650–658. [PubMed: 1332499]

[35]. Kojima T, Mitaka T, Shibata Y, Mochizuki Y. Induction and regulation of connexin26 by glucagon in primary cultures of adult rat hepatocytes. J Cell Sci. 1995; 108:2771–2780. [PubMed: 7593318]

[36]. Traub O, Look J, Dermietzel R, Brümmer F, Hülser D, Willecke K. Comparative characterization of the 21-kD and 26-kD gap junction proteins in murine liver and cultured hepatocytes. J Cell Biol. 1989; 108:1039–1051. [PubMed: 2537831]

[37]. Chu FF, Doyle D. Turnover of plasma membrane proteins in rat hepatoma cells and primary cultures of rat hepatocytes. J Biol Chem. 1985; 260:3097–3107. [PubMed: 3972818]

[38]. Traub O, Drüge PM, Willecke K. Degradation and resynthesis of gap junction protein in plasma membranes of regenerating liver after partial hepatectomy or cholestasis. Proc Natl Acad Sci U S A. 1983; 80:755–759. [PubMed: 6298773]

[39]. Spray, DC., Saez, JC., Hertzberg, EL., Dermietzel, R. Gap junctions in liver: composition, function, and regulation. The Liver: Biology and Pathobiology. Arias, IM.Boyer, JL.Fausto, N.Jakoby, DA.Schachter, DA., Shaftrits, DA., editors. Raven Press; New York: 1994. p. 951-967.

[40]. Maes M, Decrock E, Cogliati B, Oliveira AG, Marques PE, Dagli ML, Menezes GB, Mennecier G, Leybaert L, Vanhaecke T, Rogiers V, et al. Connexin and pannexin (hemi)channels in the liver. Front Physiol. 2014; 4:405. [PubMed: 24454290]

[41]. Dahlin DC, Miwa GT, Lu AY, Nelson SD. N-acetyl-p-benzoquinone imine: a cytochrome P-450-mediated oxidation product of acetaminophen. Proc Natl Acad Sci U S A. 1984; 81:1327–1331. [PubMed: 6424115]

[42]. Mitchell JR, Jollow DJ, Potter WZ, Gillette JR, Brodie BB. Acetaminophen-induced hepatic necrosis. IV. Protective role of glutathione. J Pharmacol Exp Ther. 1973; 187:211–217. [PubMed: 4746329]

[43]. Lee SS, Buters JT, Pineau T, Fernandez-Salguero P, Gonzalez FJ. Role of CYP2E1 in the hepatotoxicity of acetaminophen. J Biol Chem. 1996; 271:12063–12067. [PubMed: 8662637]

[44]. Lindros KO. Zonation of cytochrome P450 expression, drug metabolism and toxicity in liver. Gen Pharmacol. 1997; 28:191–196. [PubMed: 9013193]

[45]. McGill MR, Jaeschke H. Mechanistic biomarkers in acetaminophen-induced hepatotoxicity and acute liver failure: from preclinical models to patients. Expert Opin Drug Metabol Toxicol. 2014; 10:1005–1017.

[46]. Blazka ME, Wilmer JL, Holladay SD, Wilson RE, Luster MI. Role of proinflammatory cytokines in acetaminophen hepatotoxicity. Toxicol Appl Pharmacol. 1995; 133:43–52. [PubMed: 7597709]

[47]. Lawson JA, Farhood A, Hopper RD, Bajt ML, Jaeschke H. The hepatic inflammatory response after acetaminophen overdose: role of neutrophils. Toxicol Sci. 2000; 54:509–516. [PubMed: 10774834]

[48]. James LP, Kurten RC, Lamps LW, McCullough S, Hinson JA. Tumour necrosis factor receptor 1 and hepatocyte regeneration in acetaminophen toxicity: a kinetic study of proliferating cell nuclear antigen and cytokine expression. Basic Clin Pharmacol Toxicol. 2005; 97:8–14. [PubMed: 15943753]

[49]. Cover C, Liu J, Farhood A, Malle E, Waalkes MP, Bajt ML, Jaeschke H. Pathophysiological role of the acute inflammatory response during acetaminophen hepatotoxicity. Toxicol Appl Pharmacol. 2006; 216:98–107. [PubMed: 16781746]

[50]. Ishida Y, Kondo T, Ohshima T, Fujiwara H, Iwakura Y, Mukaida N. A pivotal involvement of IFN-gamma in the pathogenesis of acetaminophen-induced acute liver injury. FASEB J. 2002; 16:1227–1236. [PubMed: 12153990]

[51]. Jaeschke H. Glutathione disulfide formation and oxidant stress during acetaminophen-induced hepatotoxicity in mice in vivo: the protective effect of allopurinol. J Pharmacol Exp Ther. 1990; 255:935–941. [PubMed: 2262912]

[52]. Knight TR, Kurtz A, Bajt ML, Hinson JA, Jaeschke H. Vascular and hepatocellular peroxynitrite formation during acetaminophen toxicity: role of mitochondrial oxidant stress. Toxicol Sci. 2001; 62:212–220. [PubMed: 11452133]

[53]. Maes M, Cogliati B, Crespo Yanguas S, Willebrords J, Vinken M. Roles of connexins and pannexins in digestive homeostasis. Cell Mol Life Sci. 2015; 72:2809–2821. [PubMed: 26084872]

[54]. Ichai P, Samuel D. Epidemiology of liver failure. Clin Res Hepatol Gastroenterol. 2011; 35:610–617. [PubMed: 21550329]

[55]. Lee WM. Etiologies of acute liver failure. Semin Liver Dis. 2008; 28:142–152. [PubMed: 18452114]

[56]. Vinken M, Henkens T, De Rop E, Fraczek J, Vanhaecke T, Rogiers V. Biology and pathobiology of gap junctional channels in hepatocytes. Hepatology. 2008; 47:1077–1088. [PubMed: 18058951]

[57]. Mitchell JA, Lye SJ. Regulation of connexin43 expression by c-fos and c-jun in myometrial cells. Cell Commun Adhes. 2001; 8:299–302. [PubMed: 12064606]

[58]. Lefebvre DL, Piersanti M, Bai XH, Chen ZQ, Lye SJ. Myometrial transcriptional regulation of the gap junction gene, connexin-43. Reprod Fertil Dev. 1995; 7:603–611. [PubMed: 8606973]

[59]. Blazka ME, Elwell MR, Holladay SD, Wilson RE, Luster MI. Histopathology of acetaminophen-induced liver changes: role of interleukin 1 alpha and tumor necrosis factor alpha. Toxicol Pathol. 1996; 24:181–189. [PubMed: 8992608]

[60]. Fausto N, Campbell JS. The role of hepatocytes and oval cells in liver regeneration and repopulation. Mech Dev. 2003; 120:117–130. [PubMed: 12490302]

[61]. Oh SH, Hatch HM, Petersen BE. Hepatic oval 'stem' cell in liver regeneration. Semin Cell Dev Biol. 2002; 13:405–409. [PubMed: 12468240]

[62]. Ruch RJ, Trosko JE. The role of oval cells and gap junctional intercellular communication in hepatocarcinogenesis. Anticancer Res. 1999; 19:4831–4838. [PubMed: 10697596]

[63]. Zhang M, Thorgeirsson SS. Modulation of connexins during differentiation of oval cells into hepatocytes. Exp Cell Res. 1994; 213:37–42. [PubMed: 7517369]

[64]. Petersen BE, Goff JP, Greenberger JS, Michalopoulos GK. Hepatic oval cells express the hematopoietic stem cell marker Thy-1 in the rat. Hepatology. 1998; 27:433–445. [PubMed: 9462642]

[65]. Fausto N. Liver regeneration and repair: hepatocytes, progenitor cells, and stem cells. Hepatology. 2004; 39:1477–1487. [PubMed: 15185286]

[66]. Corcoran GB, Racz WJ, Smith CV, Mitchell JR. Effects of N-acetylcysteine on acetaminophen covalent binding and hepatic necrosis in mice. J Pharmacol Exp Ther. 1985; 232:864–872. [PubMed: 3973835]

[67]. Corcoran GB, Wong BK. Role of glutathione in prevention of acetaminophen-induced hepatotoxicity by N-acetyl-L-cysteine in vivo: studies with N-acetyl-D-cysteine in mice. J Pharmacol Exp Ther. 1986; 238:54–61. [PubMed: 3723405]

[68]. Knight TR, Ho YS, Farhood A, Jaeschke H. Peroxynitrite is a critical mediator of acetaminophen hepatotoxicity in murine livers: protection by glutathione. J Pharmacol Exp Ther. 2002; 303:468–475. [PubMed: 12388625]

[69]. Saito C, Zwingmann C, Jaeschke H. Novel mechanisms of protection against acetaminophen hepatotoxicity in mice by glutathione and N-acetylcysteine. Hepatology. 2010; 51:246–254. [PubMed: 19821517]

Europe PMC Funders Author Manuscripts

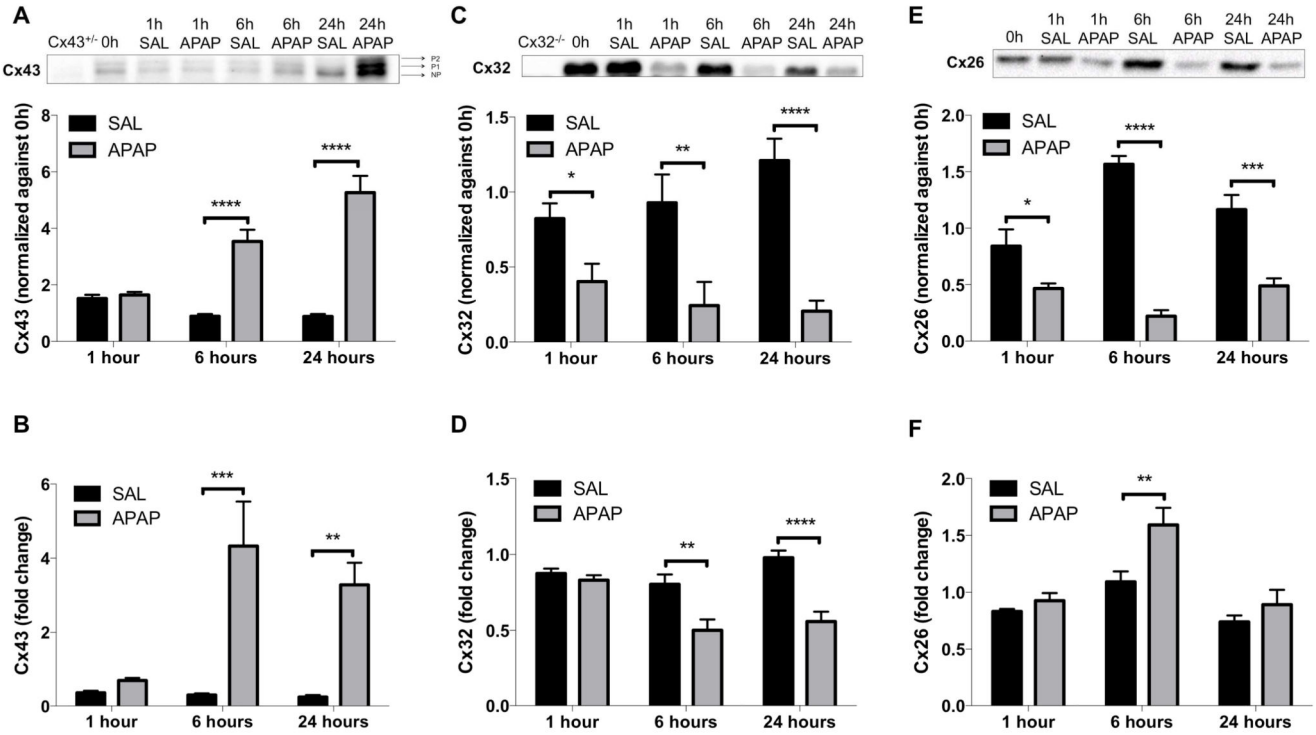

Figure 1. Alteration of hepatic connexin protein expression after APAP overdosing.

Mice (n = 5) were injected with 300 mg/kg APAP or saline (SAL) followed by sampling at different time points (*i.e.* after 0, 1, 6 and 24 hours). Hepatic protein levels of **(A)** phosphorylated (P1-P2) and non-phosphorylated (NP) Cx43, **(C)** Cx32 and **(E)** Cx26 were assessed by immunoblot analysis and expressed as relative alteration compared to untreated animals. mRNA was extracted and subjected to RT-qPCR analysis of **(B)** Cx43, **(D)** Cx32 and **(F)** Cx26. Relative alterations in mRNA levels were calculated according to the $2^{-\Delta\Delta Cq}$ formula. Data are expressed as means ± SEM with $*p \leq 0.05$ $**p \leq 0.01$, $***p \leq 0.001$ and $****p \leq 0.0001$ compared to saline at indicated time points.

Europe PMC Funders Author Manuscripts

Europe PMC Funders Author Manuscripts

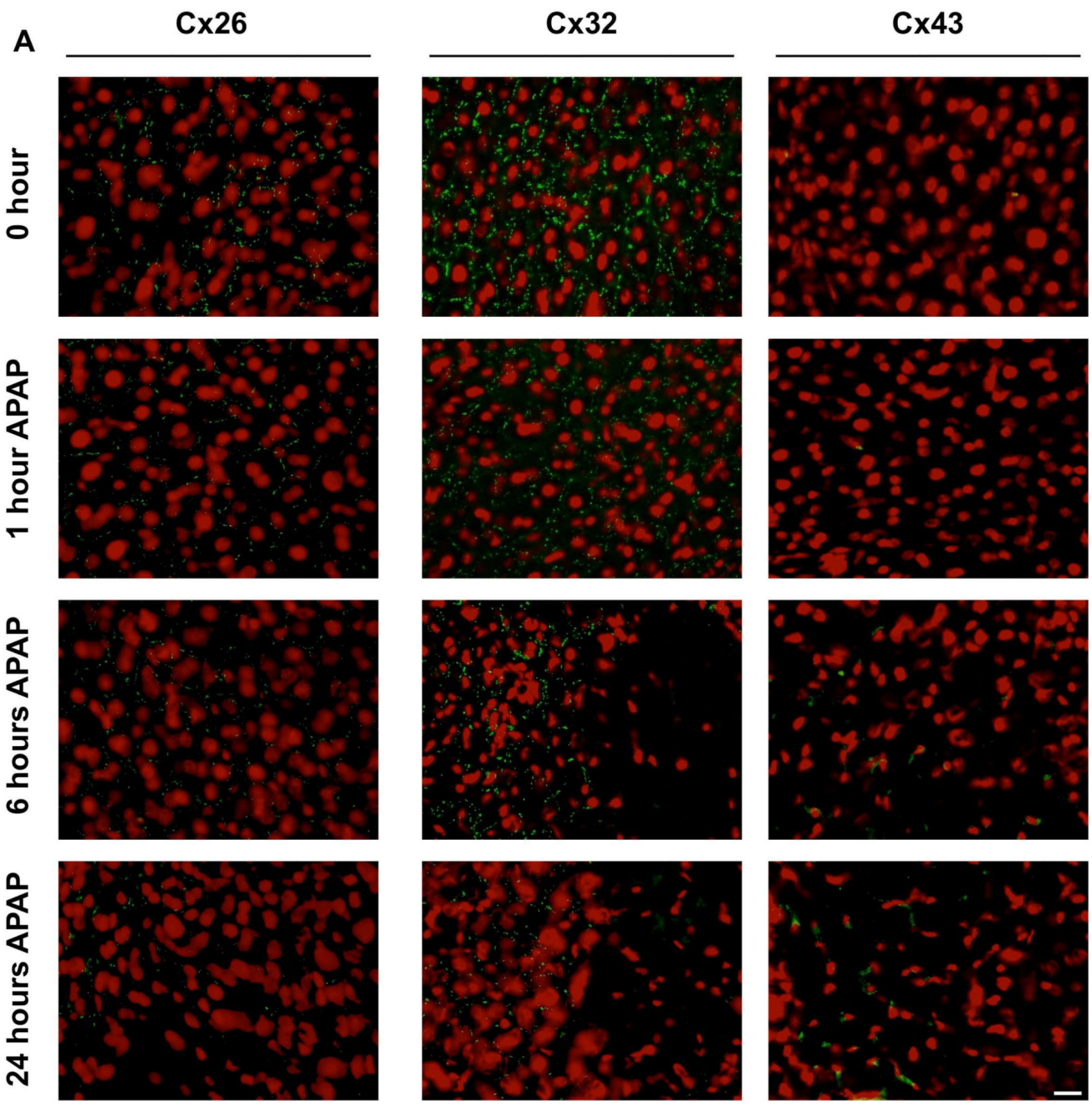

Europe PMC Funders Author Manuscripts

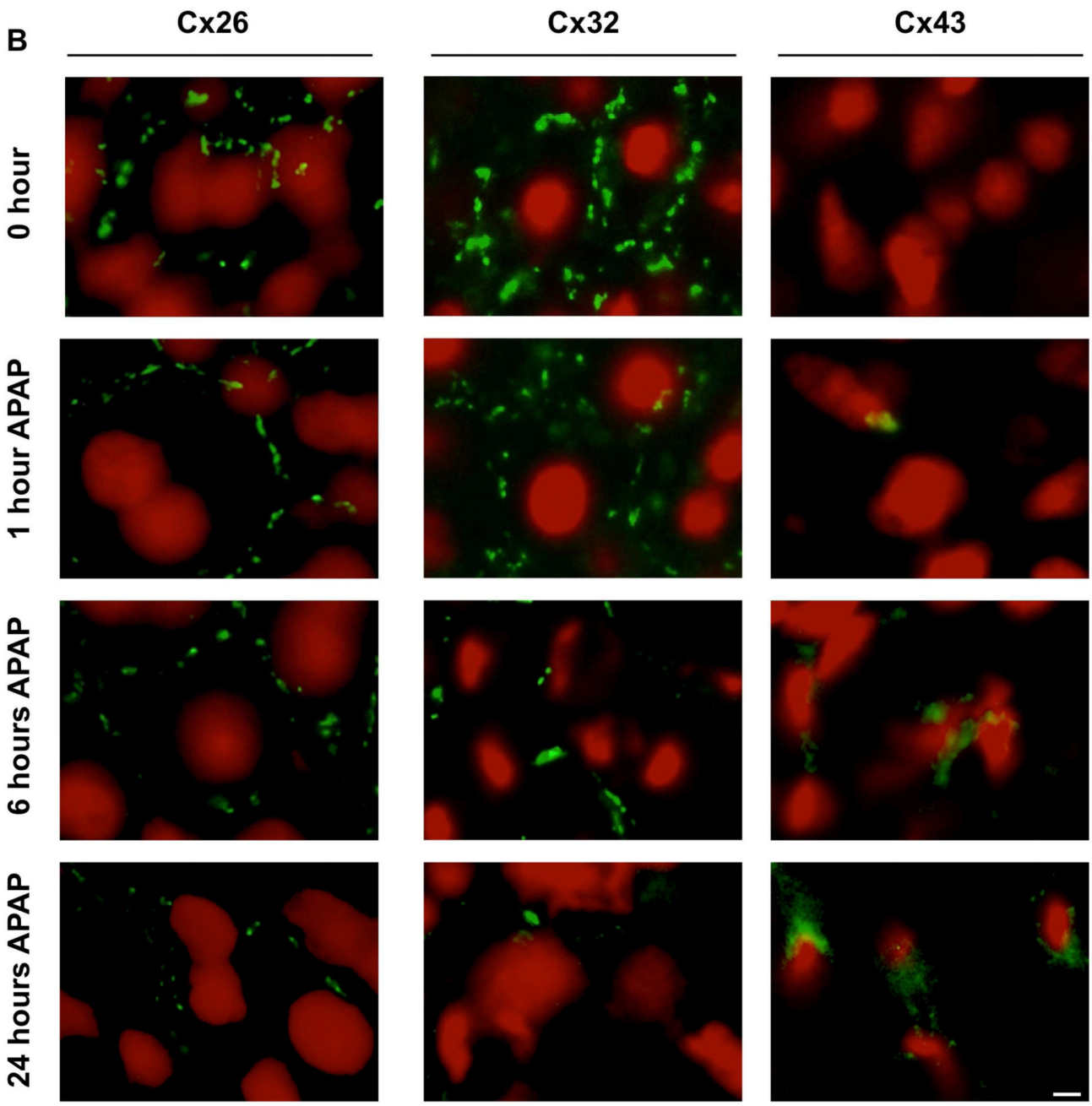

Figure 2. Alteration of hepatic connexin protein localization after APAP overdosing.

Mice (n = 5) were injected with 300 mg/kg APAP or saline (SAL) followed by sampling at different time points (*i.e.* after 0, 1, 6 and 24 hours). Hepatic localization of Cx26, Cx32 and Cx43 was assessed by immunohistochemical analysis on liver sections (green color), which was merged with nuclear propidium iodide staining (red color). The white scale bars represent **(A)** 5 μm and **(B)** 1.25 μm.

Europe PMC Funders Author Manuscripts

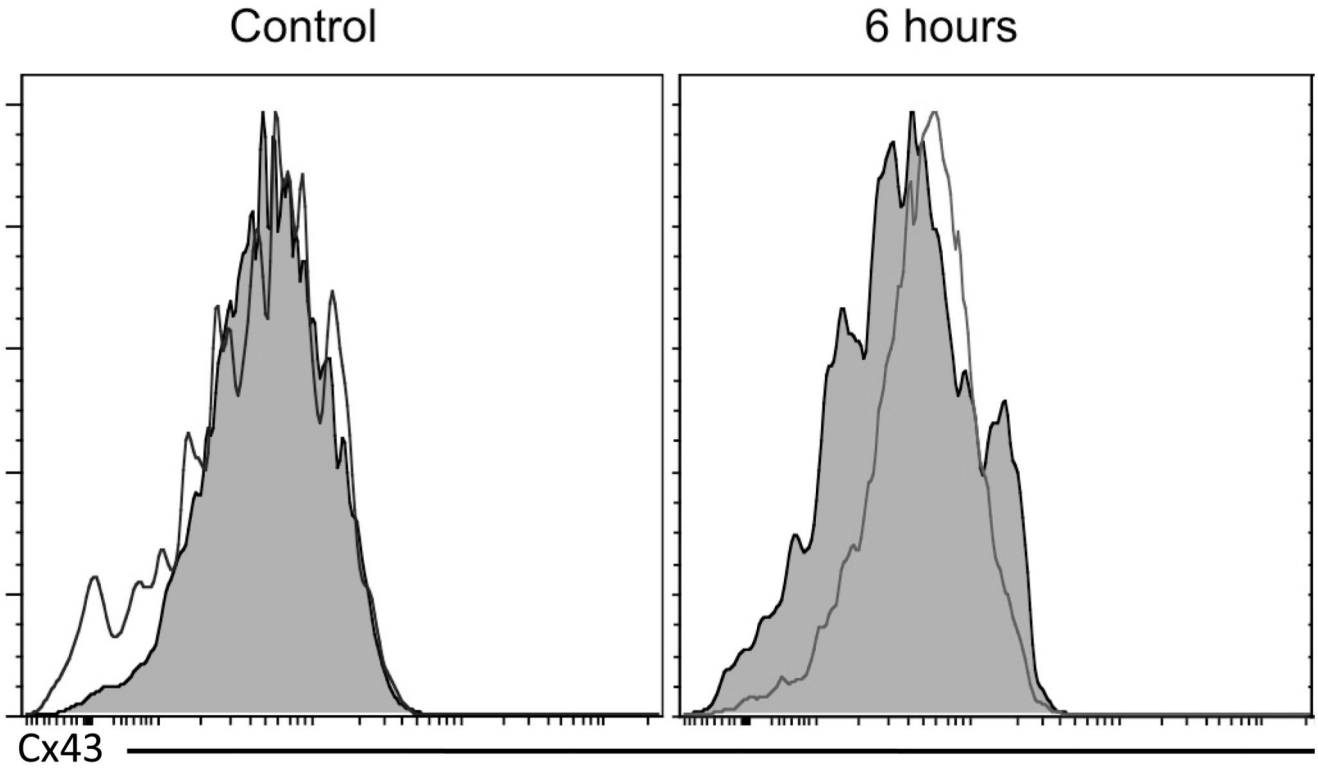

Figure 3. ***De novo*** **expression of Cx43 after APAP overdosing.**

Mice (n = 4) were injected with 300 mg/kg APAP or saline followed by sampling at 6 hours and 24 hours. Livers were subjected to flow cytometric analysis, relying on a hepatocyte-specific marker (hepaCAM) and a hematopoietic cell-specific marker (CD45). This analysis represents the Cx43 expression in the hepatocyte population, defined as hepacCAM^{+} CD45^{-} cells. The filled histogram represents the negative control with omission of primary antibody and the transparent histogram reflects the Cx43 expression.

Europe PMC Funders Author Manuscripts

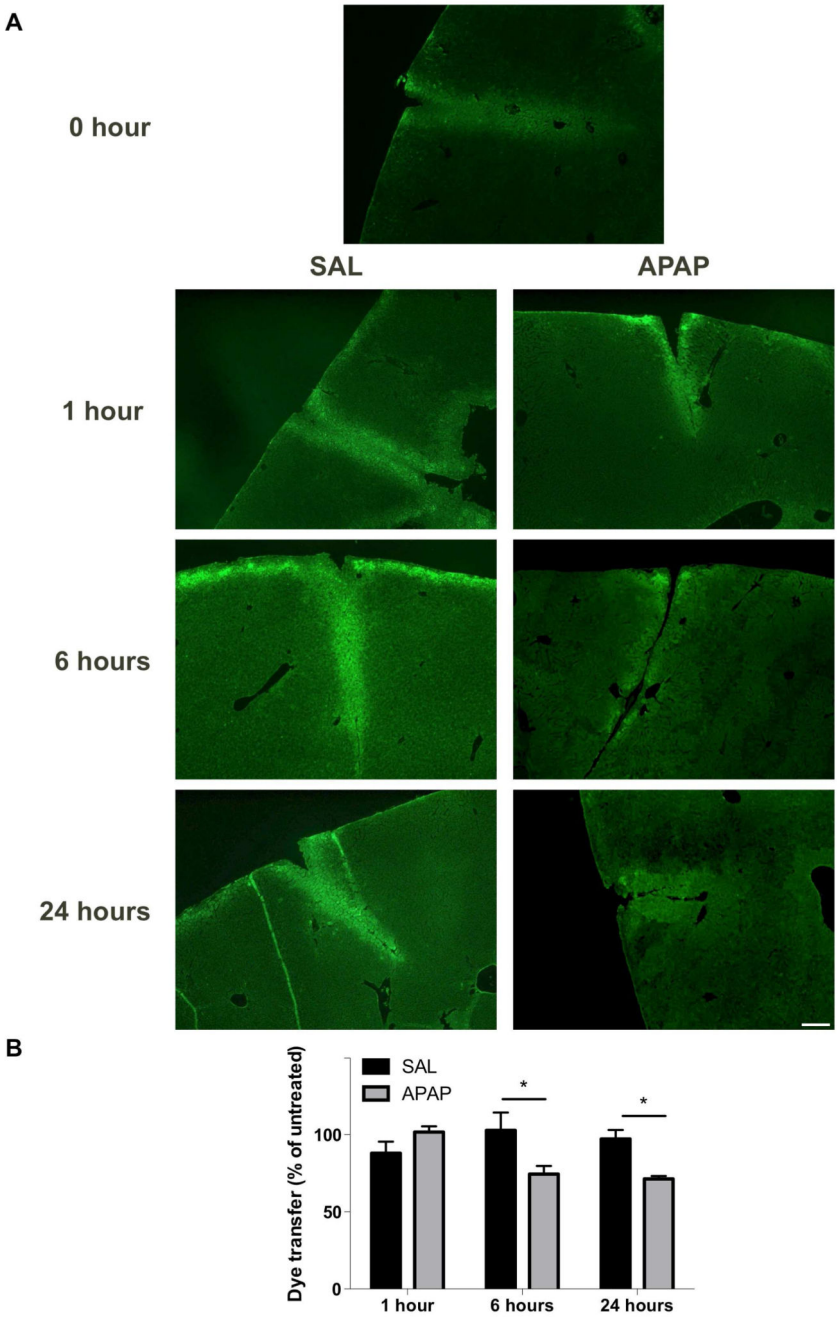

Figure 4. Alteration of hepatic GJIC after APAP overdosing.

(A) Mice (n = 5) were injected with 300 mg/kg APAP or saline (SAL) followed by assessment of GJIC by diffusion of Lucifer Yellow (green color) at different time points (*i.e.* after 0, 1, 6 and 24 hours). The white scale bar represents 50 μm. **(B)** The dye transfer ratios were quantified and normalized against untreated animals. Data are expressed as means ± SEM with $*p \leq 0.05$ compared to saline at indicated time points.

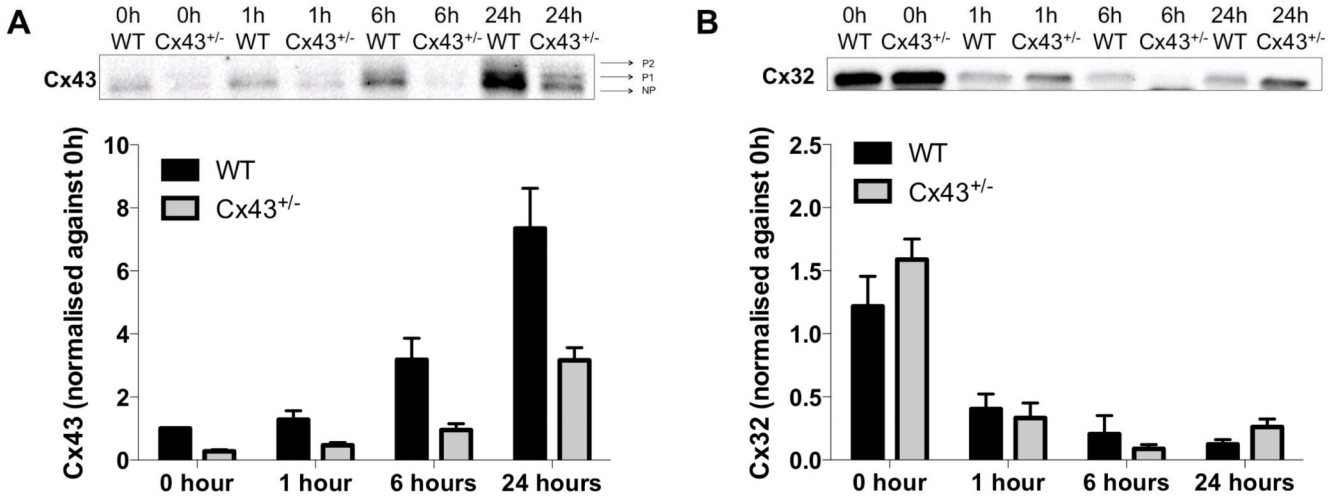

Figure 5. Effects of Cx43 ablation on connexin protein content.

WT and Cx43$^{+/-}$ mice (n = 5) were injected with 300 mg/kg APAP followed by sampling at different time points (*i.e.* after 0, 1, 6 and 24 hours). Hepatic protein levels of **(A)** phosphorylated (P1-P2) and non-phosphorylated (NP) Cx43 and **(C)** Cx32 were assessed by immunoblot analysis, and expressed as relative alteration compared to untreated WT animals. Data are expressed as means ± SEM.

Europe PMC Funders Author Manuscripts

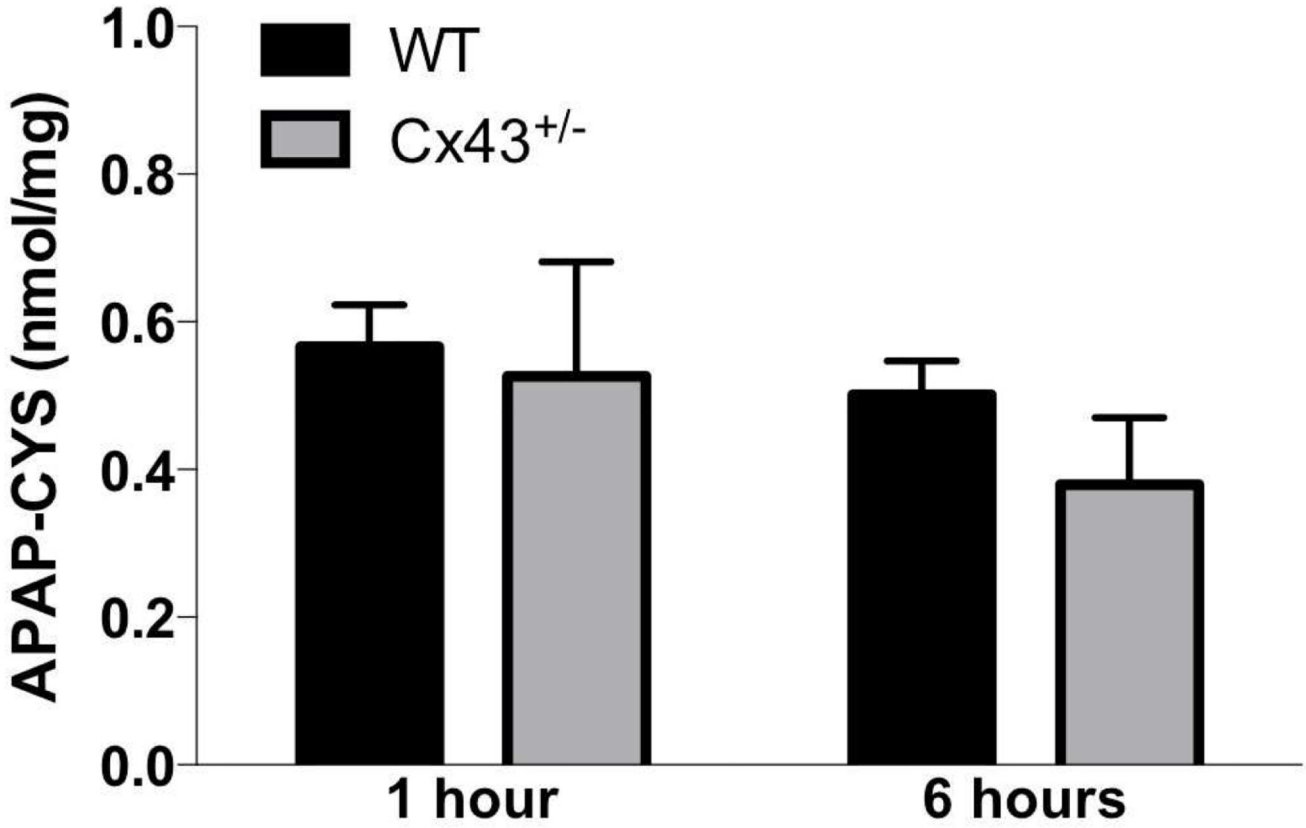

Figure 6. Effects of Cx43 ablation on APAP protein adduct formation.

WT and Cx43$^{+/-}$ mice (n = 3-8) were overdosed with 300 mg/kg APAP followed by sampling after 1 and 6 hours. The generation of reactive metabolite results in the formation of APAP-cysteine (APAP-CYS) protein adducts which were quantified by high-pressure liquid chromatography with electrochemical detection using total liver homogenate. Data were expressed as means ± SEM. No statistically significant differences were found between Cx43$^{+/-}$ and WT animals.

Europe PMC Funders Author Manuscripts

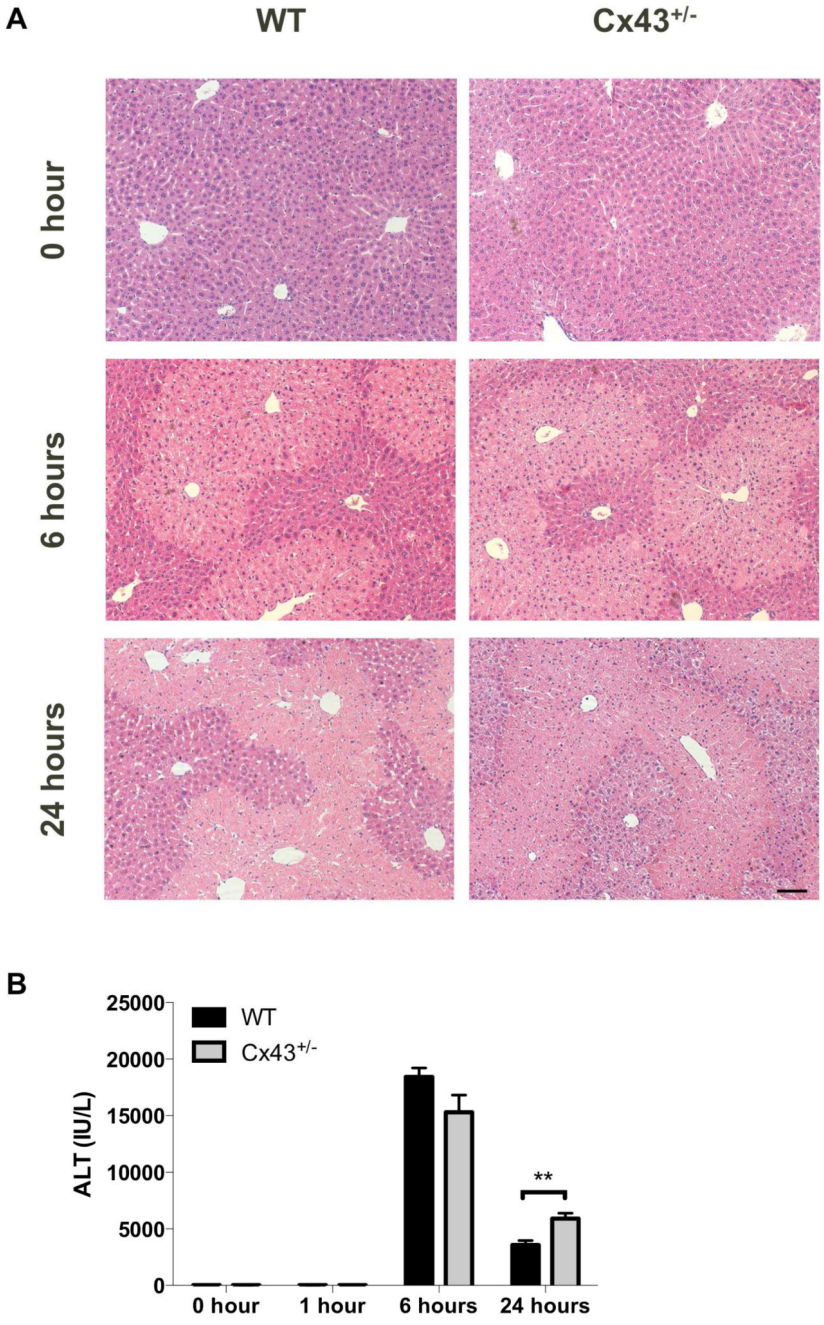

Figure 7. Effects of Cx43 ablation on APAP-induced liver cell injury.

WT and Cx43$^{+/-}$ mice (n = 5-10) were overdosed with 300 mg/kg APAP followed by sampling at different time points (*i.e.* after 0, 1, 6 and 24 hours). **(A)** Liver sections were examined microscopically with the black scale bar representing 20 μm. **(B)** Serum levels of ALT were measured at indicated time points. Data are expressed as means ± SEM with $^{**}p \leq 0.01$ compared to WT animals at indicated time points.

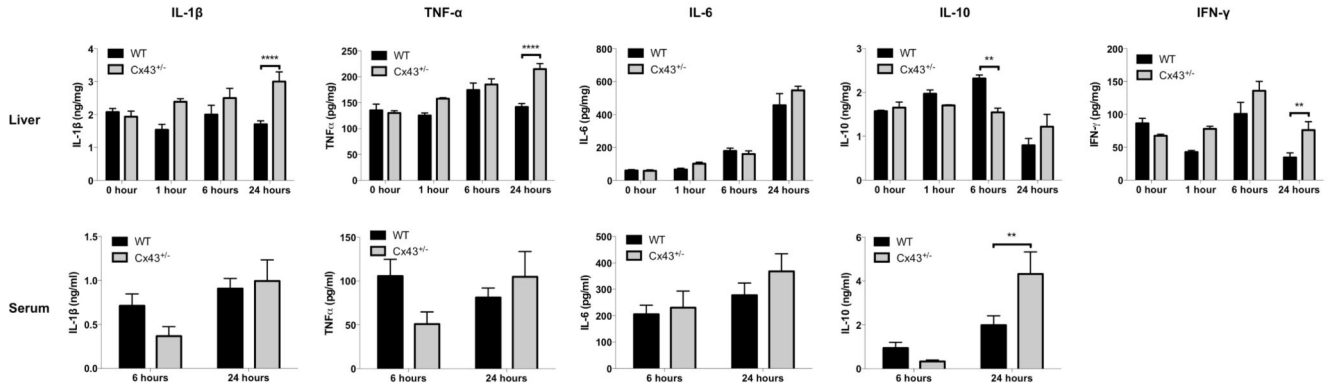

Figure 8. Effects of Cx43 ablation on APAP-induced inflammation.

WT and $Cx43^{+/-}$ mice (n = 5-10) were overdosed with 300 mg/kg APAP followed by sampling at different time points (*i.e.* after 0, 1, 6 and 24 hours). ELISA analyses of IL-1β, IL-6, IL-10, IFNγ and TNFα were performed in liver (upper panels) and serum (lower panels) samples. Data are expressed as means ± SEM with $^{**}p \leq 0.01$ and $^{****}p \leq 0.0001$ compared to WT animals at indicated time points.

Europe PMC Funders Author Manuscripts

Europe PMC Funders Author Manuscripts

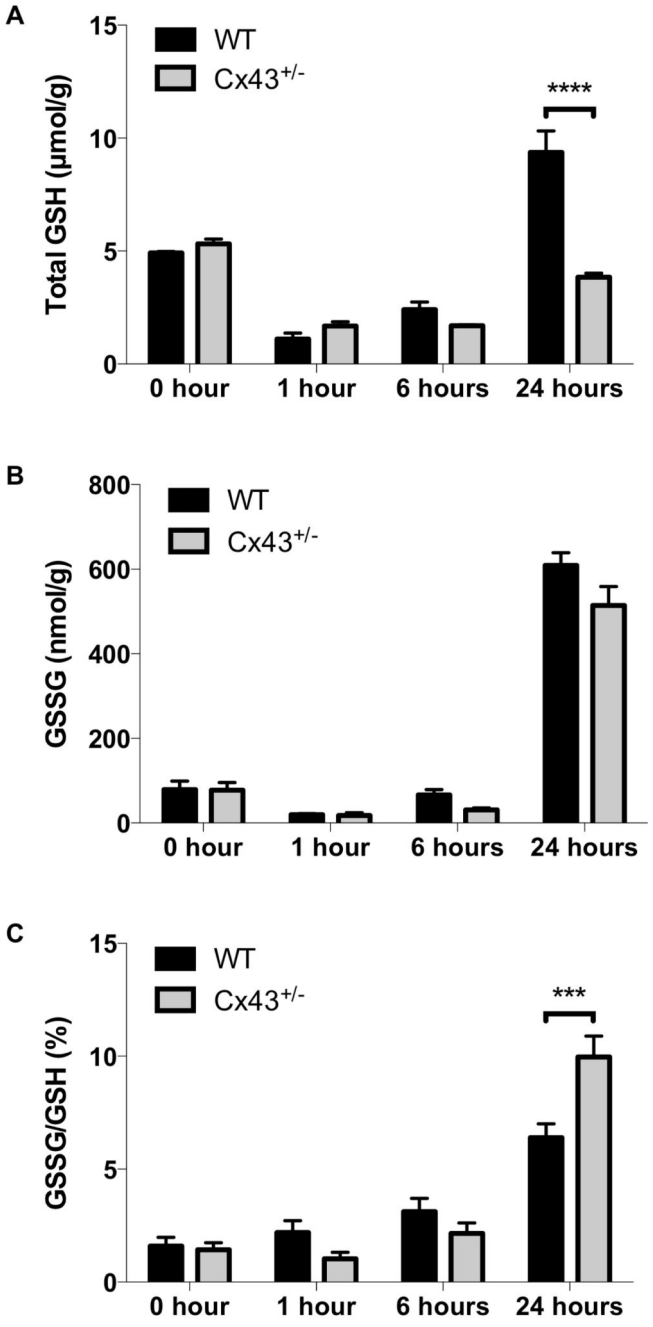

Figure 9. Effects of Cx43 ablation on APAP-induced oxidative stress.

WT and Cx43$^{+/-}$ mice (n = 3-10) were overdosed with 300 mg/kg APAP followed by sampling at different time points (*i.e.* after 0, 1, 6 and 24 hours). Hepatic levels of **(A)** GSH and **(B)** GSSG were measured in liver and **(C)** the GSSG/GSH ratio was calculated. Data are expressed as means ± SEM with ***$p \leq 0.001$ and ****$p \leq 0.0001$ compared to WT animals at indicated time points.

Europe PMC Funders Author Manuscripts

Table 1

Primers and probes for RT-qPCR analysis of connexin and candidate reference genes.

Assay identification (ID), accession number, assay location, amplicon length and exon boundary of connexin and candidate reference genes are presented (18S, 18S ribosomal RNA; Actb, β-actin; B2m, β-2-microglobulin; Gapdh, glyceraldehyde 3-phosphate dehydrogenase; Gja1, Cx43; Gjb1, Cx32; Gjb2, Cx26; Hmbs, hydroxymethylbilane synthase; Ubc, ubiquitin C).

Gene Symbol	Assay ID	Accession number	Assay location	Amplicon size (base pairs)	Exon boundary
Gjb2	Mm00433643_s1	NM_008125.3	603	72	2-2
Gjb1	Mm01950058_s1	NM_008124.2	466	65	1-1
Gja1	Mm01179639_s1	NM_010288.3	2937	168	2-2
18S	Hs99999901_s1	X03205.1	604	187	1-1
Actb	Mm00607939_s1	NM_007393.3	1233	115	6-6
B2m	Mm00437762_m1	NM_009735.3	111	77	1-2
Gapdh	Mm99999915_g1	NM_008084.2	265	107	2-3
Hmbs	Mm01143545_m1	NM_013551.2	473	81	6-7
Ubc	Mm02525934_g1	NM_019639.4	370	176	2-2